INTERNATIONAL JOURNAL FOR NUMERICAL METHODS IN FLUIDS
Int. J. Numer. Meth. Fluids **26**: 811–835 (1998)

NUMERICAL ANALYSIS OF SECONDARY INSTABILITIES OF THE INCOMPRESSIBLE BOUNDARY LAYER FLOW WITH SUCTION

JEUN-LEN WU*, SHAW-CHING SHEEN[1] AND SHENQ-YUH JAW

Department of Naval Architecture, National Taiwan Ocean University, Keelung, Taiwan, Republic of China

SUMMARY

Based on the Euler–Maclaurin formula, a compact finite difference scheme is employed to solve a two-point boundary value problem for studying the secondary instabilities of the boundary layer flow. The parametric resonance of unstable waves is explored using the Floquet method. For both subharmonic and fundamental modes, two additional Fourier terms are added in the analysis, and the spatial growth rates are determined. The effect of suction mechanism on the secondary instability waves is also investigated. From numerical experiments, it is shown that the proposed numerical scheme is very promising. © 1998 John Wiley & Sons, Ltd.

KEY WORDS: Floquet; subharmonic; fundamental; secondary instability

1. INTRODUCTION

It is well-known that the most important technique with which to postpone the occurrence of turbulent flow, which plays an important role in the viscous drag for a moving vehicle [1], is laminar flow control (LFC) in the form of suction, cooling, favorable pressure gradients and compliant walls, etc. Although the effects of these mechanisms on the primary disturbances have been studied intensively for the past few years, the effects of the secondary disturbances occurring while the amplitudes of the TS waves exceed certain threshold values have not yet been fully explored.

The pattern of the three-dimensional structure of secondary disturbances has two different types of Λ shape aligned in the spanwise. The first one was found by Klebanoff and Tidstrom [2] and is referred to as the K-type of breakdown. It is characterized by spanwise alternating peaks and valleys, or regions of enhanced and reduced wave amplitude and an associated system of streamwise vortices. Three-dimensional wave components have the same frequency as the TS wave component, so the route to transition is also referred to as the fundamental breakdown or fundamental instability. The second type was observed by Kachanov and Levchenko [3], and Thomas and Saric [4]. This type is characterized by a staggered pattern of Λ vortices, where the streamwise wavelength is twice that of the TS wave, and is usually

* Correspondence to: Department of Naval Architecture, National Taiwan Ocean University, Keelung, Taiwan, Republic of China.
[1] Present address: Department of Industrial Safety and Hygiene, Tajen Junior College of Pharmacy Yenpu, Pingtong County, Taiwan, Republic of China.

CCC 0271–2091/98/070811–25$17.50
© 1998 John Wiley & Sons, Ltd.
Received 14 August 1996
Revised 26 May 1997

referred to as subharmonic instability or the H-type of breakdown. Both K- and H-types of breakdown are, in general, called secondary instabilities. It has been shown in previous experiments [5] that the staggered Λ-shaped vortices occur at low amplitudes of TS wave, while the aligned peak–valley splitting vortices appears at higher amplitudes.

Early theoretical studies of the secondary instability rely on weakly non-linear models which are based on the interaction of some relevant primary instability modes. The results thus obtained are rarely comparable with experimental ones. The intrinsic drawback for weakly non-linear theories is that they are dominated by the characteristics of the long (viscous) time scale of the linear theory. Thus, the effects developed by the fast (inertia) time scale can not be described clearly. With the advent of the high speed computer, direct numerical simulation becomes the most direct and useful tool with which to illustrate the transition process. Spalart and Yang [6] introduced three-dimensional random disturbances to predict the spanwise structure. Kleizer and Laurien [7] modeled the subharmonic and fundamental types of instabilities. Although direct numerical simulation (DNS) confirms many experimental observations and theoretical predictions, it is extremely time consuming and complicated. An alternative is based on the fact that the secondary instability modes arise from a parametric instability of the streamwise periodic flow created by finite amplitude TS waves. Due to the fact that the governing equations have periodic coefficients, the Floquet method is easily adopted to analyze the system. Herbert [8,9] employed this parametric approach to study the subharmonic and fundamental modes of transition. The quantitative agreement with the experiments of Klebanoff on peak–valley splitting and those of Kachanov and Levchenko on staggered peak–valley is very striking. Herbert [10] also reviewed the secondary instability of incompressible flow.

In Floquet's theory, the number of the governing equations increases with increasing Fourier terms, which are used to describe the variables of the secondary instabilities. Therefore, the analyses of the secondary instability such as that of Herbert [8,9], Herbert and Bertolotti [11], EI-Hady [12], and Masad and Nayfeh [13] are almost based on the minimum number of terms to avoid the complexity in deriving and solving the governing equations. Furthermore, in order to alleviate the non-linear characteristics of the spatial stability problem by itself, the temporal stability problem is usually solved and the spatial growth rate of the disturbance is approximated by a conversion formula proposed by Bertolotti [14].

In order to understand the effect of the truncated terms on the secondary instability, this research uses four and five Fourier terms in the analysis of the subharmonic instability and in the investigation of the fundamental instability, respectively. Furthermore, the spatial stability problem is directly solved for the growth rate of the secondary instabilities and the suction effect on the secondary instabilities is studied. In general, due to numerical stiffness of both primary and secondary stability problems, a converged solution is not easy to obtain. Although there are some well-known caned codes such as SUPORT [15] and DB2PFD [16] which were developed especially for the two-point boundary value problems, the efforts to secure the converged solution require special numerical techniques such as fined-grid or very close initial conditions. To cope with this trauma, a compact finite difference numerical scheme is proposed in this research.

2. MATHEMATICAL FORMULATION

The Cartesian co-ordinates, x, y and z are used to represent the streamwise, transverse and spanwise directions, respectively. In stability analysis, each flow variable q_T,(u_T, v_T, w_T, p_T) is

© 1998 John Wiley & Sons, Ltd.

expressed by two components as $q_T = q_b + q$, where q represents the secondary instability disturbance to the basic state q_b, which is the sum of both mean flow and TS wave. The secondary instability disturbance can be obtained from

$$q_b = q_m(y) + \frac{A_{rms}}{\sqrt{2}}[q_p(y)\, e^{i\theta} + \bar{q}_p(y)\, e^{-i\theta}], \quad \text{where } \theta = \alpha x + \omega t, \tag{1}$$

where q_m stands for the mean flow variables that can be determined from the solution of the 2D laminar boundary layer equations, q_p stands for the eigenfunction satisfying the Orr–Sommerfeld equation and, α and ω represent the wave number and the frequency of TS wave, respectively. Note that

1. these functions are normalized such that the maximum root-mean-square of the streamwise velocity component, u_p, has a specified value denoted by A_{rms} and A_{rms} which are assumed locally constant, i.e. the amplitude is assumed to be very small in comparison with the disturbances.
2. Moreover, at finite amplitude A_{rms} the non-linear distortion of the primary disturbance q_p is also neglected. This assumption has been justified by the weak non-linear distortion, even at an amplitude of 10% [10].

Substituting Equation (1) into the Navier–Stoke equations, discarding the terms satisfied by q_b, and eliminating the quadratic terms of q, a three-dimensional unsteady partial differential equation for disturbance quantities $q(= u, v, p \text{ and } w)$ is then obtained:

$$\frac{\partial u}{\partial x} + \frac{\partial v}{\partial y} + \frac{\partial w}{\partial z} = 0, \tag{2}$$

$$\frac{\partial u}{\partial t} + u_b\frac{\partial u}{\partial x} + \frac{\partial u_b}{\partial x}u + v_b\frac{\partial u}{\partial y} + \frac{\partial u_b}{\partial y}v = -\frac{\partial p}{\partial x} + \frac{1}{Re}\left(\frac{\partial^2 u}{\partial x^2} + \frac{\partial^2 u}{\partial y^2} + \frac{\partial^2 u}{\partial z^2}\right), \tag{3}$$

$$\frac{\partial v}{\partial t} + u_b\frac{\partial v}{\partial x} + \frac{\partial v_b}{\partial x}u + v_b\frac{\partial v}{\partial y} + \frac{\partial v_b}{\partial y}v = -\frac{\partial p}{\partial y} + \frac{1}{Re}\left(\frac{\partial^2 v}{\partial x^2} + \frac{\partial^2 v}{\partial y^2} + \frac{\partial^2 v}{\partial z^2}\right), \tag{4}$$

$$\frac{\partial w}{\partial t} + u_b\frac{\partial w}{\partial x} + v_b\frac{\partial w}{\partial y} = -\frac{\partial p}{\partial z} + \frac{1}{Re}\left(\frac{\partial^2 w}{\partial x^2} + \frac{\partial^2 w}{\partial y^2} + \frac{\partial^2 w}{\partial z^2}\right), \tag{5}$$

where the Reynolds number $Re = U^*_\infty \delta^*/\nu^*$, and distances, velocities, time and pressure are non-dimensionalized by $\delta = \sqrt{\nu^* x^*/U^*_\infty}$, U^*_∞, δ^*/U^*_∞, and $\rho^* U^{*2}_\infty$, respectively. The boundary conditions are given by

$$u = v = w = 0 \quad \text{at} \quad y = 0, \tag{6}$$

and

$$u, v, p, w \to 0, \quad \text{as} \quad y \to \infty. \tag{7}$$

Equations (2)–(5) are linear, and their coefficients are independent of z and periodic in both the t- and x-direction. Therefore, based upon the Floquet theory, the solution is written as:

$$(u, v, p) = e^{\gamma x + \sigma t}(\eta_1, \eta_3, \eta_4 + \text{complex conjugate}) \cos \beta z, \tag{8}$$

$$w = e^{\gamma x + \sigma t}(\eta_5 + \text{complex conjugate}) \sin \tag{9}$$

where γ and σ are called the characteristic exponents and β represents the spanwise wave number. Since η_k $(k = 1, 3, 4, 5)$ is periodic in x and t, we express η_k as

© 1998 John Wiley & Sons, Ltd.

$$\eta_k = \sum_{n=-\infty}^{\infty} \zeta_k^{n/2}(y)\, e^{in\theta/2}, \quad \begin{cases} n = \text{odd}; & \text{for subharmonic instability.} \\ n = \text{even}; & \text{for fundamental instability.} \end{cases} \tag{10}$$

It is obvious that the accuracy of the parametric resonance wave solution depends on the numbers of Fourier terms chosen, and one additional term will result in one more set of Equations (2)–(5). Consequently, in order to reduce the complexity and to save some CPU time, most contemporary researches are limited to a minimum of two Fourier terms for subharmonic instability and three Fourier terms for fundamental instability [17]. To understand the effect of truncation error in the analysis of the secondary instability, two additional terms are added to this study. By so doing, the disturbances q for subharmonic instability can be written as

$$(u, du/dy, v, p) = e^{\gamma x + \sigma t}[\zeta_k^{1/2} e^{i\theta/2} + \zeta_k^{-1/2} e^{-i\theta/2} + \zeta_k^{3/2} e^{i3\theta/2} + \zeta_k^{-3/2} e^{-i3\theta/2}] \cos \beta z, \quad k = 1, \ldots, 4, \tag{11}$$

$$(w, dw/dy) = e^{\gamma x + \sigma t}[\zeta_k^{1/2} e^{i\theta/2} + \zeta_k^{-1/2} e^{-i\theta/2} + \zeta_k^{3/2} e^{i3\theta/2} + \zeta_k^{-3/2} e^{-i3\theta/2}] \sin \beta z, \quad k = 5, 6, \tag{12}$$

and the disturbances for fundamental instability are

$$(u, du/dy, v, p) = e^{\gamma x + \sigma t}[\zeta_k^0 + \zeta_k^1 e^{i\theta} + \zeta_k^{-1} e^{-i\theta} + \zeta_k^2 e^{i2\theta} + \zeta_k^{-2} e^{-i2\theta}] \cos \beta z, \quad k = 1, \ldots, 4, \tag{13}$$

$$(w, dw/dy) = e^{\gamma x + \sigma t}[\zeta_k^0 + \zeta_k^1 e^{i\theta} + \zeta_k^{-1} e^{-i\theta} + \zeta_k^2 e^{i2\theta} + \zeta_k^{-2} e^{-i2\theta}] \sin \beta z, \quad k = 5, 6. \tag{14}$$

Substituting Equations (11) and (12) into (2)–(5), and equating the coefficients of $e^{i\theta/2}$ and $e^{i3\theta/2}$ on both sides, the resulting equations can be written as a system of 12 coupled first-order differential equations in terms of $\zeta_n^{1/2}$ and $\zeta_n^{3/2}$:

$$\frac{d\zeta_n^{1/2}}{dy} = \sum_{k=1}^{6} F_{nk}\zeta_k^{1/2} + \bar{F}_{nk}\zeta_k^{-1/2} + G_{nk}\zeta_k^{3/2}, \quad n = 1, \ldots, 6, \tag{15}$$

$$\frac{d\zeta_n^{3/2}}{dy} = \sum_{k=1}^{6} \hat{F}_{nk}\zeta_k^{1/2} + \hat{G}_{nk}\zeta_k^{3/2}, \quad n = 1, \ldots, 6. \tag{16}$$

The coefficients F_{nk}, $\bar{F}_{nk}$, G_{nk}, $\hat{F}_{nk}$ and $\hat{G}_{nk}$ are given in Appendix A, where $\bar{\zeta}_k$ is the complex conjugate of ζ_k.

The boundary conditions are then transformed into

$$\zeta_n^{1/2} = \zeta_n^{3/2} = 0, \quad \text{at } y = 0,\ n = 1, 3, 5, \tag{17}$$

$$\zeta_n^{1/2} \text{ and } \zeta_n^{3/2} \to 0, \quad \text{as } y \to \infty,\ n = 1, \ldots, 6. \tag{18}$$

Likewise, for the fundamental instability, 18 coupled first-order differential equations in terms of variables ζ_n^0, ζ_n^1 and ζ_n^2 are obtained. They are given as follows:

$$\frac{d\zeta_n^0}{dy} = \sum_{k=1}^{6} \tilde{H}_{nk}\zeta_k^0 + \tilde{F}_{nk}\zeta_k^1 + \tilde{\bar{F}}_{nk}\bar{\zeta}_k^1, \quad n = 1, \ldots, 6, \tag{19}$$

$$\frac{d\zeta_n^1}{dy} = \sum_{k=1}^{6} H_{nk}\zeta_k^0 + F_{nk}\zeta_k^1 + G_{nk}\zeta_k^2, \quad n = 1, \ldots, 6, \tag{20}$$

$$\frac{d\zeta_n^2}{dy} = \sum_{k=1}^{6} \hat{F}_{nk}\zeta_k^1 + \hat{G}_{nk}\zeta_k^2, \quad n = 1, \ldots, 6, \tag{21}$$

© 1998 John Wiley & Sons, Ltd.

where the coefficients, $\tilde{H}_{nk}, \tilde{F}_{nk}, \tilde{\tilde{F}}_{nk}, H_{nk}, F_{nk}, G_{nk}, \hat{F}_{nk}, \hat{G}_{nk}$, are given in Appendix B. The boundary conditions read

$$\zeta_n^0 = \zeta_n^1 = \zeta_n^2 = 0, \quad \text{at } y = 0, \ n = 1, 3, 5, \tag{22}$$

$$\zeta_n^0, \zeta_n^1 \text{ and } \zeta_n^2 \to 0, \quad n = 1, 6, \text{ as } y \to \infty. \tag{23}$$

2.1. Mean flow

For the flow over a two-dimensional curved body, the non-dimensional boundary layer equations take the form of

$$\frac{\partial u_m}{\partial x} + \frac{\partial v_m}{\partial y} = 0 \tag{24}$$

$$u_m \frac{\partial u_m}{\partial x} + v_m \frac{\partial u_m}{\partial y} = u_e \frac{du_e}{dx} + \frac{\partial^2 u_m}{\partial y^2}. \tag{25}$$

The boundary conditions are given below,

$$v_m = v_w, \quad u_m = 0, \quad \text{at } y = 0, \text{ and } u_m = u_e(x) \quad \text{as } y \to \infty, \tag{26}$$

where

$$\begin{cases} (x, y) = (x^*, y^* \sqrt{Re_L})/L^*, (u_m, v_m) = (u_m^*, v_m^* \sqrt{Re_L})/u_{m\infty}^* \\ Re_L = \rho_\infty^* u_{m\infty}^* L^*/\mu_\infty^*. \end{cases}$$

Variables with subscripts represent the quantities of the free stream flow: $u_e(x)$ and v_w denotes inviscid solution and the normal velocity at wall, respectively.

Applying the Görtler transformation shown below

$$\xi(x) = \int_0^x u_e \, dx, \qquad \eta(x, y) = \frac{u_e(x) y}{\sqrt{2\xi}},$$

the governing equations become

$$2\xi F_\xi + V_\eta + F = 0, \tag{27}$$

$$2\xi F F_\xi + V F_\eta - F_{\eta\eta} + \beta(F^2 - 1) = 0 \tag{28}$$

where

$$F(\xi, \eta) = \frac{u_m(x, y)}{u_e(x)}, \qquad V(\xi, \eta) = \frac{\sqrt{2\xi}}{u_e} (v_w(\xi) + \sqrt{2\xi} \eta_x F).$$

The parameter $\beta = 2\xi/u_e \, du_e/d\xi$ represents the pressure gradient along the surface.

The boundary conditions become

$$F = 0, \quad V = \frac{\sqrt{2\xi}}{u_e} V_w(\xi) \quad \text{at } y = 0, \quad \text{and} \quad F = 1 \quad \text{as } y \to \infty. \tag{29}$$

We now consider the flow over a flat plate. Let V be constant at $y = 0$, meaning that the suction $V_w(\xi)$ is distributed as a function of the downstream.

2.2. TS waves (primary instability)

The procedure for deriving the governing equations of the primary instability problem is very similar to that of the secondary instability problems. A system of equations for the 2D TS waves is

© 1998 John Wiley & Sons, Ltd.

$$\frac{d\zeta_n}{dy} = \sum_{m=1}^{4} F_{nm}(y, \alpha, \omega, Re)\zeta_m, \quad n = 1,\ldots, 4, \tag{30}$$

where $[\zeta_1, \zeta_2, \zeta_3, \zeta_4] = [u_p, du_p/dy, v_p, p_p]$ and

$$F_{nm} = \begin{bmatrix} 0 & 1 & 0 & 0 \\ \alpha^2 - iRe\Omega & 0 & Reu'_m & i\alpha Re \\ -i\alpha & 0 & 0 & 0 \\ 0 & -i\alpha/Re & -\alpha^2/Re + i\Omega & 0 \end{bmatrix} \tag{31}$$

where $\Omega = \omega - \alpha u_m$. Equation (30) is in fact the well-known Orr–Sommerfeld equation. Since the y-derivative of the mean flow velocity is zero outside the boundary layer thickness, the asymptotic boundary conditions are derived and expressed as

$$\sum_{m=1}^{4} A_{nm}\zeta_m = 0 \text{ at } y = 0, \quad \text{and} \quad \sum_{m=1}^{4} B_{nm}\zeta_m = 0 \text{ at } y = y_{\max}, \quad \text{for } n = 1, 2, \tag{32}$$

where the $y_{\max}$ is specified with the magnitude equal to or larger than the boundary layer thickness, and

$$[A]_{2\times 4} = \begin{bmatrix} 1 & 0 & 0 & 0 \\ 0 & 0 & 1 & 0 \end{bmatrix}, \qquad [B]_{2\times 4} = \begin{bmatrix} 0 & -i & -\Omega_c/\alpha & Re \\ -\Omega Re/\alpha & -i\sqrt{\Omega_c}/\alpha & -\sqrt{\Omega_c} & Re \end{bmatrix}$$

where $\Omega_c = \alpha^2 - i\Omega Re$.

3. NUMERICAL METHOD

With the homogenous boundary conditions, the homogeneous system of Equations (15)–(18) or (19)–(23) is basically an eigenvalue problem. The system has a non-trivial solution for certain combinations of σ, γ, β, ω, A_{rms}, u_m and Re, satisfying a dispersion relation,

$$\gamma = \gamma(\sigma, \beta, \omega, A_{\text{rms}}, u_m, Re). \tag{33}$$

For temporal stability, we set $\gamma = 0$, so that σ_r gives the growth rate and σ_i represents a frequency shift from $\omega/2$. For spatial stability, we set $\sigma = 0$, so that γ_r gives the growth rate and γ_i represents a wave number shift from $\alpha/2$. For synchronized secondary instability waves, usually called tuned mode, we have $\sigma_i = 0$ and $\gamma_i = 0$. Since the growth rate of the tuned mode is usually larger than that of the detuned mode, only the tuned mode is considered in the present work.

The governing equations of both primary and secondary stability problems become more and more stiff as Re is increased. A famed SUPORT code [15] was developed to deal with the stiffness problem through Gram–Schmidt renormalization techniques during the integration, in order to determine both compressible and incompressible stability problems. However, as the problem becomes stiff, the fine grid requires a tremendous amount of CPU time owing to the renormalization of the eigenfunctions. Recently, a subroutine DB2PFD of IMSL using the second-order finite differences [16] has been developed for a non-linear two-point boundary value problem. The code has been used by Masad and Nayfeh [13] in dealing with the instability problem. DB2PFD is accurate and considerably faster than SUPORT, especially at low Reynolds number. However, when the problem becomes stiffer, DB2PFD usually produces a diverged message even with fine grid used, or may even obtain a wrong solution. Wu

© 1998 John Wiley & Sons, Ltd.

[18] has applied the Euler–Maclaurin formula and used the finite difference method to analyze the stability of a compressible mixing layer numerically. The solutions can attain to the fourth-order accuracy in the y-direction, which offers much more accuracy for the first- and second-derivatives of the mean flow which is required for the stability analysis. Therefore, an attempt is made to extend this numerical scheme in order to solve the secondary instability problem, which is much more complex than the primary instability problem. Certainly, the mean flow and the primary stability can also be solved based on this scheme. For simplicity, only the numerical procedure for solving the subharmonic instability is described here.

The prime hub of the scheme is based on the application of the Euler–Maclaurin formula to the system, such as

$$(\vec{\psi}_j - \vec{\psi}_{j-1}) - \frac{h_j}{2}(\vec{\psi}'_j + \vec{\psi}''_{j-1}) + \frac{h_j^2}{12}(\vec{\psi}''_j - \psi''_{j-1}) + O(h_j^5) = 0, \tag{34}$$

where j represents the grid point index in the y-direction. $\vec{\psi}$ acts as a vector of 12 components, i.e. $(\psi_1, \ldots, \psi_6, \psi_7, \ldots, \psi_{12}) = (\zeta_1^{1/2}, \ldots, \zeta_6^{1/2}, \zeta_1^{3/2}, \ldots, \zeta_6^{3/2})$, which stand for the variables of the system. $\vec{\psi}'_j$ represents the first derivative of $\vec{\psi}$ with respect to y. $\vec{\psi}''$ is determined by taking the derivative of Equations (15) and (16) directly. They are given by

$$\frac{\mathrm{d}^2\zeta_n^{1/2}}{\mathrm{d}y^2} = \sum_{k=1}^{6} f_{nk}\zeta_k^{1/2} + \bar{f}_{nk}\bar{\zeta}_k^{1/2} + g_{nk}\zeta_k^{3/2} + \bar{g}_{nk}\bar{\zeta}_k^{3/2}, \tag{35}$$

$$\frac{\mathrm{d}^2\zeta_n^{3/2}}{\mathrm{d}y^2} = \sum_{k=1}^{6} \hat{f}_{nk}\zeta_k^{1/2} + \hat{\bar{f}}_{nk}\bar{\zeta}_k^{1/2} + \hat{g}_{nk}\zeta_k^{3/2}. \tag{36}$$

for the subharmonic mode, where

$$f_{nk} = \frac{\mathrm{d}F_{nk}}{\mathrm{d}y} + \sum_{l=1}^{6} [F_{nl}F_{lm} + \bar{F}_{nl}\bar{F}_{lm} + G_{nl}\hat{F}_{lm}],$$

$$\bar{f}_{nk} = \frac{\mathrm{d}\bar{F}_{nk}}{\mathrm{d}y} + \sum_{l=1}^{6} [F_{nl}\bar{F}_{lm} + \bar{F}_{nl}\bar{F}_{lm}],$$

$$g_{nk} = \frac{\mathrm{d}G_{nk}}{\mathrm{d}y} + \sum_{l=1}^{6} [F_{nl}G_{lm} + G_{nl}\hat{G}_{lm}],$$

$$\bar{g}_{nk} = \sum_{l=1}^{6} \bar{F}_{nl}\bar{G}_{lm}, \qquad \hat{f}_{nk} = \frac{\mathrm{d}\hat{F}_{nk}}{\mathrm{d}y} + \sum_{l=1}^{6} [\hat{F}_{nl}F_{lm} + \hat{G}_{nl}\hat{F}_{lm}],$$

$$\hat{\bar{f}}_{nk} = \sum_{l=1}^{6} \hat{F}_{nl}\bar{F}_{lm}, \qquad \hat{g}_{nk} = \frac{\mathrm{d}\hat{G}_{nk}}{\mathrm{d}y} + \sum_{l=1}^{6} [\hat{F}_{nl}G_{lm} + \hat{G}_{nl}G_{lm}].$$

The system of the equations has to be entered into another system of equations in terms of real variables prior to numerical calculations. Thus, with some manipulation, the transformed real-variable equations of the system become

© 1998 John Wiley & Sons, Ltd.

$$
\begin{Bmatrix}
\frac{d\psi_1^r}{dy} \\
\frac{d\psi_1^i}{dy} \\
\vdots \\
\frac{d\psi_6^r}{dy} \\
\frac{d\psi_6^i}{dy} \\
\frac{d\psi_7^r}{dy} \\
\frac{d\psi_7^i}{dy} \\
\vdots \\
\frac{d\psi_{12}^r}{dy} \\
\frac{d\psi_{12}^i}{dy}
\end{Bmatrix}
=
\begin{bmatrix}
F_{11}^r + \bar{F}_{11}^r & -F_{11}^i + \bar{F}_{11}^i & \cdots & F_{16}^r + \bar{F}_{16}^r & -F_{16}^i + \bar{F}_{16}^i & G_{11}^r & -G_{11}^i & \cdots & G_{16}^r & -G_{16}^i \\
F_{11}^i + \bar{F}_{11}^i & F_{11}^r - \bar{F}_{11}^r & \cdots & F_{16}^i + \bar{F}_{16}^i & F_{16}^r - \bar{F}_{16}^r & G_{11}^i & G_{11}^r & \cdots & G_{16}^i & G_{16}^r \\
\vdots & \vdots & \vdots & \vdots & \vdots & \vdots & \vdots & \vdots & \vdots & \vdots \\
F_{61}^r + \bar{F}_{61}^r & -F_{61}^i + \bar{F}_{61}^i & \cdots & F_{66}^r + \bar{F}_{66}^r & -F_{66}^i + \bar{F}_{66}^i & G_{61}^r & -G_{61}^i & \cdots & G_{66}^r & -G_{66}^i \\
F_{61}^i + \bar{F}_{61}^i & F_{61}^r - \bar{F}_{61}^r & \cdots & F_{66}^i + \bar{F}_{66}^i & F_{66}^r - \bar{F}_{66}^r & G_{61}^i & G_{61}^r & \cdots & G_{66}^i & G_{66}^r \\
\tilde{F}_{11}^r & -\tilde{F}_{11}^i & \cdots & \tilde{F}_{16}^r & -\tilde{F}_{16}^i & \tilde{G}_{11}^r & -\tilde{G}_{11}^i & \cdots & \tilde{G}_{16}^r & -\tilde{G}_{16}^r \\
\tilde{F}_{11}^i & \tilde{F}_{11}^r & \cdots & \tilde{F}_{16}^i & \tilde{F}_{16}^r & \tilde{G}_{11}^i & \tilde{G}_{11}^r & \cdots & \tilde{G}_{16}^i & \tilde{G}_{16}^r \\
\vdots & \vdots & \vdots & \vdots & \vdots & \vdots & \vdots & \vdots & \vdots & \vdots \\
\tilde{F}_{61}^r & -\tilde{F}_{61}^i & \cdots & \tilde{F}_{66}^r & -\tilde{F}_{66}^i & \tilde{G}_{61}^r & -\tilde{G}_{61}^i & \cdots & \tilde{G}_{66}^r & -\tilde{G}_{66}^i \\
\tilde{F}_{61}^i & -\tilde{F}_{61}^i & \cdots & \tilde{F}_{66}^r & -\tilde{F}_{66}^i & G_{61}^r & -\tilde{G}_{61}^i & \cdots & \tilde{G}_{66}^i & \tilde{G}_{66}^r
\end{bmatrix}
=
\begin{Bmatrix}
\psi_1^r \\
\psi_1^i \\
\vdots \\
\psi_6^r \\
\psi_6^i \\
\psi_7^r \\
\psi_7^i \\
\vdots \\
\psi_{12}^r \\
\psi_{12}^i
\end{Bmatrix}
$$

$$
= [\Gamma]_{24*24}\{\psi_1^r, \psi_1^i, \ldots, \psi_6^r, \psi_6^i, \psi_7^i, \ldots, \psi_{12}^r, \psi_{12}^i\}^T = [\Gamma]_{24*24}\{\vec{\phi}\}_{24*1}^T, \tag{37}
$$

where $\psi_n = \psi_n^r + i\psi_n^i$. Similarly, Equations (35) and (36) are expressed in a real-variable system of equations as

© 1998 John Wiley & Sons, Ltd.

$$
\begin{Bmatrix}
\dfrac{d^2\psi_1^r}{dy^2} \\
\dfrac{d^2\psi_1^i}{dy^2} \\
\vdots \\
\dfrac{d^2\psi_6^r}{dy^2} \\
\dfrac{d^2\psi_6^i}{dy^2} \\
\dfrac{d^2\psi_7^r}{dy^2} \\
\dfrac{d^2\psi_7^i}{dy^2} \\
\vdots \\
\dfrac{d^2\psi_{12}^r}{dy^2} \\
\dfrac{d^2\psi_{12}^i}{dy^2}
\end{Bmatrix}
=
\begin{bmatrix}
f_{11}^r+\bar{f}_{11}^r & -f_{11}^i+\bar{f}_{11}^i & \cdots & f_{16}^r+\bar{f}_{16}^r & -f_{16}^i+\bar{f}_{16}^i & g_{11}^r+\bar{g}_{11}^r & -g_{11}^i+\bar{g}_{11}^i & \cdots & g_{16}^r+\bar{g}_{16}^r & -g_{16}^i+\bar{g}_{16}^i \\
f_{11}^i+\bar{f}_{11}^i & f_{11}^r-\bar{f}_{11}^r & \cdots & f_{16}^i+\bar{f}_{16}^i & f_{16}^r-\bar{f}_{16}^r & g_{11}^i+\bar{f}_{11}^i & g_{11}^r-\bar{g}_{11}^r & \cdots & g_{16}^i+\bar{f}_{16}^i & g_{16}^r-\bar{g}_{16}^r \\
\vdots & \vdots & \vdots & \vdots & \vdots & \vdots & \vdots & \vdots & \vdots & \vdots \\
f_{61}^r+\bar{f}_{61}^r & -f_{61}^i+\bar{f}_{61}^i & \cdots & f_{66}^r+\bar{f}_{66}^r & -f_{66}^i+\bar{f}_{66}^i & g_{61}^r+\bar{f}_{61}^r & -g_{61}^i+\bar{g}_{61}^i & \cdots & g_{66}^r+\bar{f}_{66}^r & -g_{66}^i+\bar{g}_{66}^i \\
f_{61}^i+\bar{f}_{61}^i & f_{61}^r-\bar{f}_{61}^r & \cdots & f_{66}^i+\bar{f}_{66}^i & f_{66}^r-\bar{f}_{66}^r & g_{61}^i+\bar{f}_{61}^i & g_{61}^r-\bar{g}_{61}^r & \cdots & g_{66}^i+\bar{f}_{66}^i & g_{66}^r-\bar{g}_{66}^r \\
\tilde{f}_{11}^r+\tilde{\bar{f}}_{11}^r & -\tilde{f}_{11}^i+\tilde{\bar{f}}_{11}^i & \cdots & \tilde{f}_{16}^r+\tilde{\bar{f}}_{16}^r & -\tilde{f}_{16}^i+\tilde{\bar{f}}_{16}^i & \tilde{g}_{11}^r & -\tilde{g}_{11}^i & \cdots & \tilde{g}_{16}^r & -\tilde{g}_{16}^i \\
\tilde{f}_{11}^i+\tilde{\bar{f}}_{11}^i & \tilde{f}_{11}^r-\tilde{\bar{f}}_{11}^r & \cdots & \tilde{f}_{16}^i+\tilde{\bar{f}}_{16}^i & \tilde{f}_{16}^r-\tilde{\bar{f}}_{61}^r & \tilde{g}_{11}^i & \tilde{g}_{11}^r & \cdots & \tilde{g}_{16}^i & \tilde{g}_{16}^r \\
\vdots & \vdots & \vdots & \vdots & \vdots & \vdots & \vdots & \vdots & \vdots & \vdots \\
\tilde{f}_{61}^r+\tilde{\bar{f}}_{61}^r & -\tilde{f}_{61}^i+\tilde{\bar{f}}_{61}^i & \cdots & \tilde{f}_{66}^r+\tilde{\bar{f}}_{66}^r & -\tilde{f}_{66}^i+\tilde{\bar{f}}_{66}^i & \tilde{g}_{61}^r & -\tilde{g}_{61}^i & \cdots & \tilde{g}_{66}^r & -\tilde{g}_{66}^i \\
\tilde{f}_{61}^i+\tilde{\bar{f}}_{61}^i & \tilde{f}_{61}^r-\tilde{\bar{f}}_{61}^r & \cdots & \tilde{f}_{66}^i+\tilde{\bar{f}}_{66}^i & \tilde{f}_{66}^r-\tilde{\bar{f}}_{66}^r & \tilde{g}_{61}^i & \tilde{g}_{61}^r & \cdots & \tilde{g}_{66}^i & \tilde{g}_{66}^r
\end{bmatrix}
\begin{Bmatrix}
\psi_1^r \\
\psi_1^i \\
\vdots \\
\psi_6^r \\
\psi_6^i \\
\psi_7^r \\
\psi_7^i \\
\vdots \\
\psi_{12}^r \\
\psi_{12}^i
\end{Bmatrix}
\tag{38}
$$

$$
= [A_{nk}]_{24*24}\{\phi\}_{24}^T*].
$$

© 1998 John Wiley & Sons, Ltd.

In the calculation '$n_{\max}$' grid points in the y-direction are generated. The first point $j=1$ represents the location at the wall. The last point $j=n_{\max}$ is located outside the boundary layer. Substituting the vector $\vec{\psi}_n$, Equations (37) and (38) into (34), the system of the equations can be expressed in a matrix form,

$$[D]_j\vec{\phi}_{j-1}+[E]_j\vec{\phi}_j=\vec{0}, \quad 2\le j\le n_{\max}, \tag{39}$$

where

$$[D]_j=-[I]-\frac{h_j}{2}[\Gamma]_{j-1}-\frac{h_j^2}{12}[\Lambda]_{j-1},$$

$$[E]_j=[I]-\frac{h_j}{2}[\Gamma]_j+\frac{h_j^2}{12}[\Lambda]_j.$$

In Equation (39) there are $24*(n_{\max}-1)$ equations for $24*n_{\max}$ unknown variables. For a system which can be solved, 24 additional equations must be derived from the boundary conditions. From the boundary condition (17) at the wall, there are 12 equations:

$$[A]_{12*24}\{\vec{\phi}\}=0, \tag{40}$$

where the elements of matrix $[A]$ are zero except that elements $A_{1,1}=A_{2,2}=A_{3,5}=A_{4,6}=A_{5,9}=A_{6,10}=A_{7,13}=A_{8,14}=A_{9,17}=A_{10,18}=A_{11,21}=A_{12,22}=1$.

The boundary condition (18) at $j=n_{\max}$ gives the other 12 equations. Since all the derivatives of mean flow are zero at or outside the boundary layer, the asymptotic boundary conditions can be derived in a matrix form

$$\begin{bmatrix}[B]_{6*12} & [0]_{6*12}\\ [0]_{6*12} & [B]_{6*12}\end{bmatrix}\{\vec{\phi}\}_{24*1}=\{0\}, \tag{41}$$

where the non-zero element of matrix $[B]$ is displayed in Appendix C.

With some manipulation, Equations (39)–(41) are combined and rewritten in a block tridiagonal system. The Newton–Raphson scheme is employed for eigenvalue searching. The procedure for obtaining the algebraic system of equations for the fundamental mode is the same, except 12 additional variables are used at each grid point.

4. VERIFICATION OF THE CODE

The mean flow, TS wave and the secondary instability are all calculated based on the proposed numerical scheme. The compact finite difference numerical scheme has second-order accuracy when the first two terms of (34) are used. It benefits without deriving and solving Equations (35) and (36), but suffers from a loss of accuracy of the numerical solution. The symbols 2ND and 4TH denote the numerical code using two terms of (34) and three other terms. All the computations were done using a 486 personal computer.

4.1. Mean flow and TS waves

In the calculation of the mean flow, the solutions obtained from 2ND and 4TH are compared and the expenditure of CPU time is shown. The Blasius profile is chosen. Let

© 1998 John Wiley & Sons, Ltd.

$\eta_{\max} = 6.0$. Firstly, for different meshpoints N, the y-derivative of velocity profile, $\partial u_m/\partial\eta|_{\eta=0}$ is computed. Since no exact solution of $\partial u_m/\partial\eta|_{\eta=0}$ at the wall can be found, $\partial u_m/\partial\eta|_{\eta=0}$ obtained at $N = 1601$ is presumed to be the exact numerical solution, which is $\partial u_m/\partial\eta|_{\eta=0} = 0.46960049176$.

Surprisingly, the result obtained by 4TH at $N = 41$ is even closer to the exact solution than that determined by 2ND at $N = 801$, and the CPU time consumed by both codes shows less difference at each respective N (Table I). As mentioned earlier, to increase the accuracy of solutions to the stability problem, highly accurate distributions of the first and second y-derivative of the mean flow velocity are required. Obviously, from Table I, 4TH proves to be a highly efficient numerical method to determine the mean flow and for both first and second derivatives of the velocity profile with respect to y.

To compare the difference in solving the TS wave problem with both codes, the Blasius profile was chosen as the mean flow, with the Reynolds number $Re_{\delta_1} = 100\,000$ (where δ_1 is the

Table I. $\partial u_m/\partial\eta|_{\eta=0}$ for various values of N

N	2ND	CPU	4TH	CPU
41	0.46943275711	0″:88	0.46960055514	0″:94
101	0.46957363752	1″:27	0.46960049337	1″:37
401	0.46959881318	2″:51	0.46960049177	2″:68
801	0.46960007211	6″:26	0.46960049176	6″:86

Table II. α obtained from 2ND for various values of N

N	α	CPU	$\lvert\alpha-\alpha_e\rvert/\alpha_e$
41	$0.572474 * 10^{-1} - i0.516940 * 10^{-2}$	4″:45	$0.28 * 10^{-1}$
101	$0.560032 * 10^{-1} - i0.374870 * 10^{-2}$	8″:57	$0.42 * 10^{-2}$
201	$0.558301 * 10^{-1} - i0.362768 * 10^{-2}$	14″:72	$0.10 * 10^{-2}$
401	$0.557880 * 10^{-1} - i0.359981 * 10^{-2}$	27″:24	$0.25 * 10^{-3}$
801	$0.557775 * 10^{-1} - i0.359298 * 10^{-2}$	52″:46	$0.64 * 10^{-4}$

Table III. α obtained from 4TH for various values of N

N	α	CPU	$\lvert\alpha-\alpha_e\rvert/\alpha_e$
41	$0.558044 * 10^{-1} - i0.352327 * 10^{-2}$	5″:44	$0.46 * 10^{-3}$
101	$0.557747 * 10^{-1} - i0.358895 * 10^{-2}$	9″:99	$0.90 * 10^{-5}$
201	$0.557742 * 10^{-1} - i0.359061 * 10^{-2}$	17″:24	$0.40 * 10^{-6}$
401	$0.557741 * 10^{-1} - i0.359071 * 10^{-2}$	31″:48	$0.80 * 10^{-8}$
801	$0.557741 * 10^{-1} - i0.359072 * 10^{-2}$	60″:42	0

© 1998 John Wiley & Sons, Ltd.

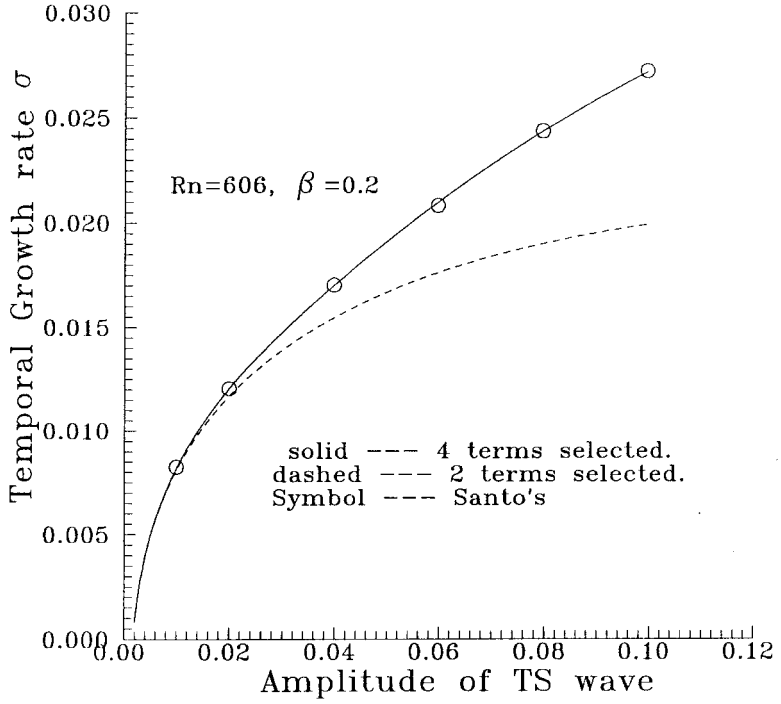

Figure 1. Comparison of subharmonic growth rates between two and four terms of the Fourier series for TS waves $\alpha = 0.20338$, $\omega = 0.075161$.

displacement thickness), $\omega = 0.008$, and the initial guess of $\alpha = 0.462609 * 10^{-1} - i0.75200 * 10^{-2}$. Similarly, at $N = 1601$, $\alpha_e = 0.557741 * 10^{-1} - i0.3.5902 * 10^{-2}$ obtained from 4TH are assumed as the exact solution for this flow condition.

From Tables II and III, at each grid point the CPU time consumed by 4TH and 2ND shows little difference, but solutions obtained by 4TH are much closer to the numerical exact solution with less grid point, which can be observed between 4TH at $N = 101$ and 2ND at $N = 801$. The error of mean flow solutions from 2ND at $N = 41$ causes large error of stability solution shown in Table II.

The solution obtained using SUPORT with $N = 101$ is $\alpha_e = 0.557741 * 10^{-1} - i0.359073 * 10^{-2}$. The CPU time is 5′:49″:77. Similarly, the solution obtained by DB2PFD with $N = 101$ is $\alpha_e = 0.557741 * 10^{-1} - i0.359073 * 10^{-2}$. The CPU time is 5′:18″:07. At $N = 401$, CPU times used by SUPORT and DB2PFD are around tenfold more than 4TH.

From this comparison, it shows that the scheme developed in the study is highly reliable. The CPU time used by SUPORT or DB2PFD increases rapidly as Reynolds number increases because of a much stiffer problem; moreover, the DB2PFD usually shows a diverged message at higher Reynolds number. However, the proposed scheme performs very well, with no apparent increase of CPU time as Reynolds number increases. The steadiness of the numerical scheme, which is rarely affected by the Reynolds number, might be attributed to its backward finite difference [19] while applying the Euler–Maclaurin formula.

© 1998 John Wiley & Sons, Ltd.

4.2. Subharmonic mode

Figure 1 shows the distribution of the temporal growth rate σ versus A_{rms} for $Re = 606$ and $\beta = 0.2$. The results of two- and four-Fourier term analyses are compared with Santo's work [17], in which the growth rate was computed using the spectral collocation techniques. In the figure, we found that the difference between the results of two and four terms becomes evident when $A_{\text{rms}} > 0.02$. The error was 21.8% at $A_{\text{rms}} = 0.06$ and 36% at $A_{\text{rms}} = 0.1$. Furthermore, the results using four terms show an excellent agreement with Santo's results. Therefore, unless the results were specified by something else, the subharmonic modes in the work are determined using four Fourier terms.

To understand the accuracy of the transformation, $\gamma = \sigma/C_{ph}$, proposed by Bertolottii [14], the distributions of both temporal and spatial growth rates versus A_{rms} were plotted in Figure 2. The figure shows that the transformed growth rate agrees well with the calculated one when $A_{\text{rms}} < 0.04$. However, substantial differences appeared for an increasing A_{rms}. Therefore, the discrepancy between both will be larger than the results shown in Figure 2 if the temporal growth rate is calculated using two Fourier terms.

4.3. Fundamental mode

At $Re = 606$ and $\beta = 0.2$ the distribution of the temporal growth rate of the fundamental wave against A_{rms} is plotted in Figure 3. In the figure we found that the term-truncated effect

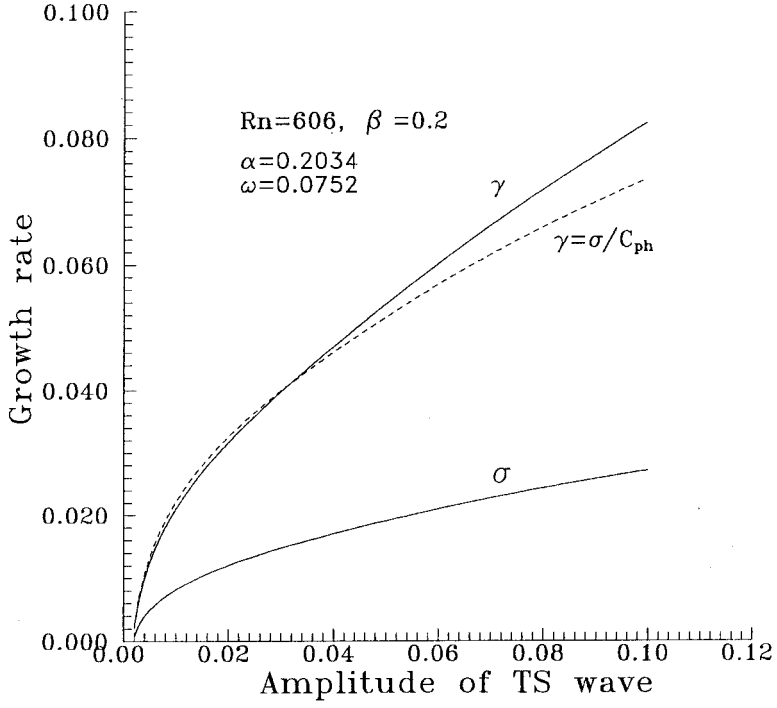

Figure 2. Comparison of subharmonic growth rates between the calculated values and values from transformation $\gamma = \sigma/C_{ph}$.

© 1998 John Wiley & Sons, Ltd.

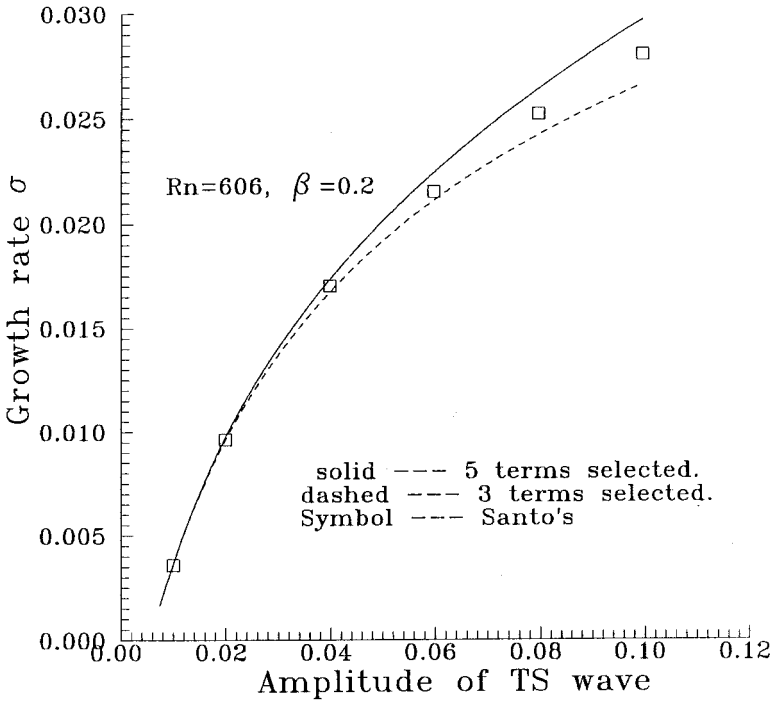

Figure 3. Comparison of fundamental growth rates between three and five terms of the Fourier series for TS wave $\alpha = 0.20338$, $\omega = 0.075161$.

on the growth rates is not pronounced for $A_{\text{rms}} < 0.02$. The error becomes clear when $A_{\text{rms}} > 0.02$. The error is about 11.3% at $A_{\text{rms}} = 0.1$. The discrepancy of the present results compared with Santo's is attributed to the four Fourier terms that he used.

The distribution of the spatial growth rate against the wave number for three different A_{rms} are plotted in Figure 4. The results are compared with Masad and Nayfeh [13], who used three Fourier terms and adopted DB2PFD to solve the fundamental stability problem. Similar to the temporal stability problem shown in Figure 3, the rare difference between the results obtained using three and five Fourier terms, as shown in Figure 3, is expected at small A_{rms}. Moreover, for $A_{\text{rms}} = 0.025$ at high spanwise numbers, the growth rate determined using five terms is larger than that obtained using three terms. Also, the present results using three Fourier terms agree well with those of Masad and Nayfeh.

Herbert [10] stated the reasonable assumption that non-linear distortion of the primary disturbance shape mode could be neglected even at $A_{\text{rms}} = 10\%$. However, the current numerical results available were all obtained at a range of amplitude A_{rms} no more than 0.01 [12,13]. They have shown that under this amplitude range, the minimum Fourier terms are sufficient for the analysis of the secondary instability. Certainly, our results also agree with their conclusions as given in Figures 1, 3 and 4. The secondary instability for amplitudes higher than this range has not been described in contemporary literature, possibly because if more Fourier terms were chosen the calculation of the growth rate would become more complex and difficult.

© 1998 John Wiley & Sons, Ltd.

5. RESULTS AND DISCUSSION

5.1. Mean flow

The velocity distributions u_m of the 2D boundary layer flow for different suctions $V = 0.05$, 0.0, -0.5 and -0.1, are shown in Figure 5. As the suction is increased, the velocities at a region near the wall are apparently increased. This phenomenon illustrates that with suction mechanism, the increasing kinetic energy of the fluid particles near wall would prevent the flow from separation, and the flow could be more stable downstream.

5.2. TS wave

The neutral curves for four different suctions are displayed in Figure 6. At a fixed disturbance frequency there are two points intersected by the neutral curve. Between these two points is the region of unstable waves. The figure illustrates that the suction mechanism causes a higher critical Reynolds number at which unstable TS waves start to grow, and the delayed occurrence of the unstable waves leads to the late occurrence of turbulence. Interestingly, suction affects the first neutral point rather than the second neutral point, which is apparently idle for suction.

5.3. Secondary instabilities

The distributions of spatial growth rates of both the subharmonic and the fundamental modes versus the spanwise wave number corresponding to $A_{\mathrm{rms}} = 0.01$, 0.02 and 0.04,

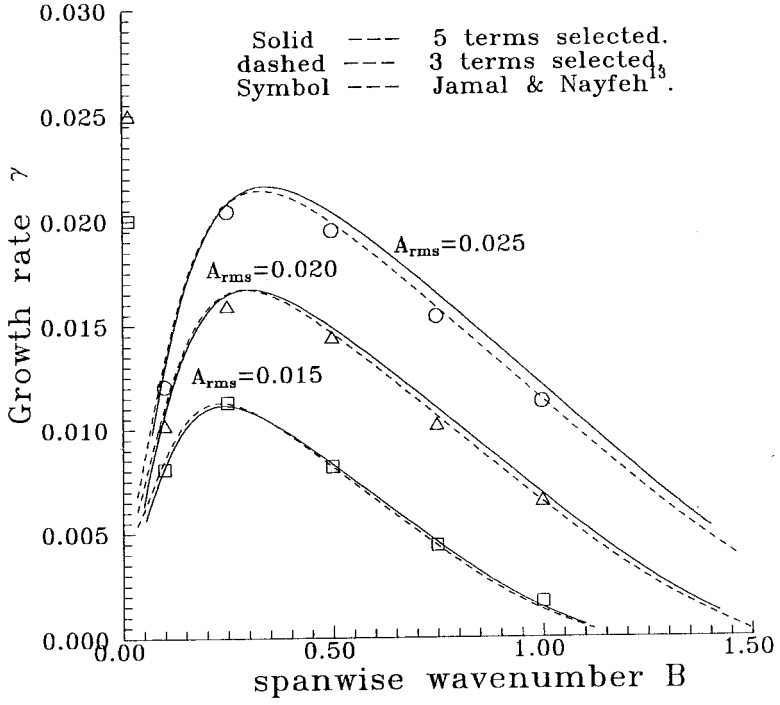

Figure 4. Comparison of fundamental growth rates between three terms of the Fourier series for TS wave $F = 90 * 10^{-6}$ and $Rn = 600$.

© 1998 John Wiley & Sons, Ltd.

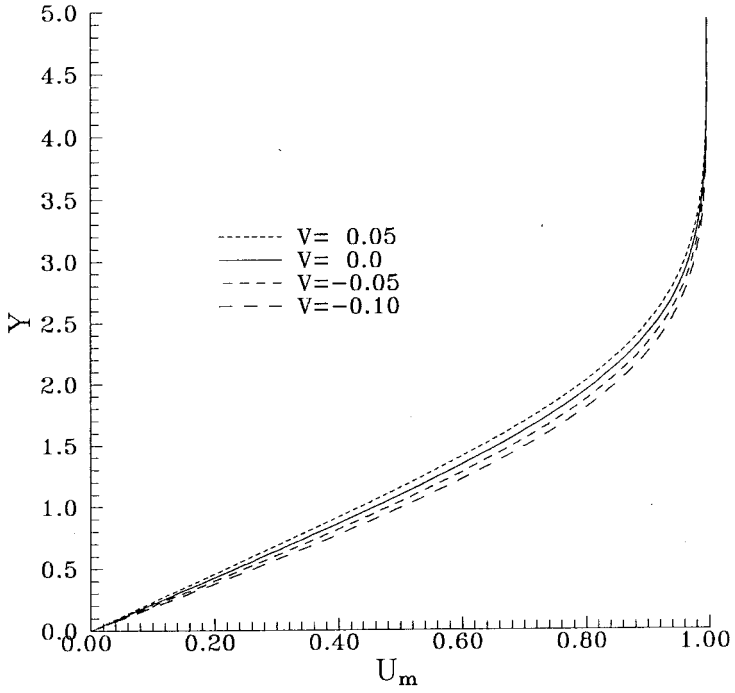

Figure 5. Distribution of mean flow u-component for different suctions.

respectively, are presented in Figures 7–9. The small growth rate at larger suction illustrates that the suction mechanism is capable of stabilizing the secondary instability. Furthermore, the range of the spanwise wave number of secondary instability is narrowed as the suction is increased. Since the subharmonic mode generally has a larger growth rate than the fundamental mode for these three different A_{rms}, the H-type of breakdown would be more likely to occur than the K-type of breakdown in the process of developing into turbulent flow.

At $Re = 600$ and $F = 90 * 10^{-6}$, the maximum growth rate of both the subharmonic and the fundamental modes was investigated among, γ–B at a fixed A_{rms}, and the variations of the maximum growth rate against A_{rms} for four different values of V are shown in the Figure 10. In each case, the maximum growth rate of the subharmonic mode is larger than that of the fundamental mode for all A_{rms} and the difference between them is evident at small A_{rms}. Furthermore, the maximum growth rate of the subharmonic mode varies almost linearly with A_{rms}. This also applies to the fundamental mode, while $A_{\text{rms}} > 0.025$.

At a fixed A_{rms} the effects of suction on the maximum growth rate of both the subharmonic and the fundamental modes are calculated and shown in Figure 11. Again, it is shown that the applied suction produces lower maximum growth rates of the secondary instabilities. The K-type of breakdown with $V < -0.075$ is unlikely to appear if $A_{\text{rms}} < 0.01$. Moreover, the maximum growth rate of both secondary instabilities decreases almost linearly as the suction is increased. For the same flow conditions as above, the spanwise wave numbers of the maximum growth rates against the suction for different A_{rms} are presented in Figure 12. The spanwise wave number at the maximum growth rate of the subharmonic mode shows little change with the suction, and the fundamental mode also shows the same tendency, except at $A_{\text{rms}} = 0.01$. Meanwhile, the figure illustrates that a larger A_{rms} will cause the secondary instabilities with maximum growth rate to occur at a high spanwise wave numbers.

© 1998 John Wiley & Sons, Ltd.

6. CONCLUSION

A highly efficient finite difference scheme is proposed to solve the two-point boundary value problem arising from boundary layer equations, Orr–Sommerfeld equations and the secondary instability equations. With this numerical scheme, the stiffness of the present problems caused by the Reynolds number is easily tackled.

Two additional Fourier terms, other than those used by other researchers, are employed in the calculation of both subharmonic and fundamental waves. The results illustrate that as the TS wave amplitude increases, additional terms should be considered in the analysis of parametric resonant waves. In particular, for the subharmonic wave, the resulting difference between using four and two Fourier terms has 36% error for $A_{\mathrm{rms}} = 10\%$. The accuracy of the numerical results in the analysis of the secondary instability is achieved for the price of obtaining more complex system equations. In the present study, four Fourier terms for the subharmonic mode and five Fourier terms for the fundamental mode are believed to be sufficient for most of the practical problems.

Suction mechanism not only suppresses the occurrence of both the subharmonic and the fundamental waves, but also shrinks the region of unstable spanwise wave numbers. The maximum growth rates of both the subharmonic and the fundamental waves vary almost linearly with the TS wave amplitude when suction is fixed. The spanwise wave number of the maximum growth rate remains nearly constant as the suction is changed. Moreover, at high TS wave amplitude, the spanwise wave numbers of the maximum growth rate of both the subharmonic and the fundamental waves are very close. On the whole, the flows seem to be vulnerable to the subharmonic mode that emerges as the principal mechanism of transition.

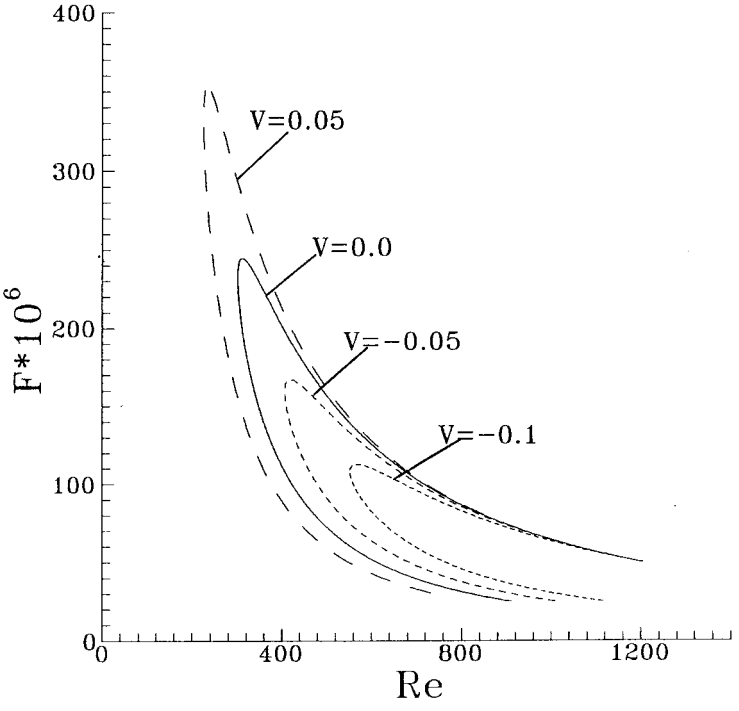

Figure 6. Neutral curves for the 2D TS wave in the F–R domain for four different suctions.

© 1998 John Wiley & Sons, Ltd.

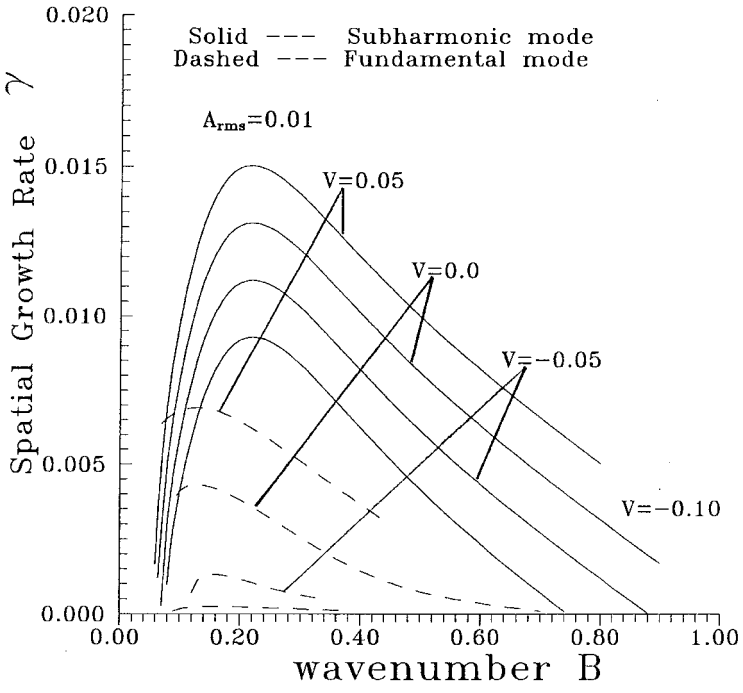

Figure 7. The variation of spatial growth rate γ against wave number B for different suction at $F = 90 * 10^{-6}$ and $Re = 600$.

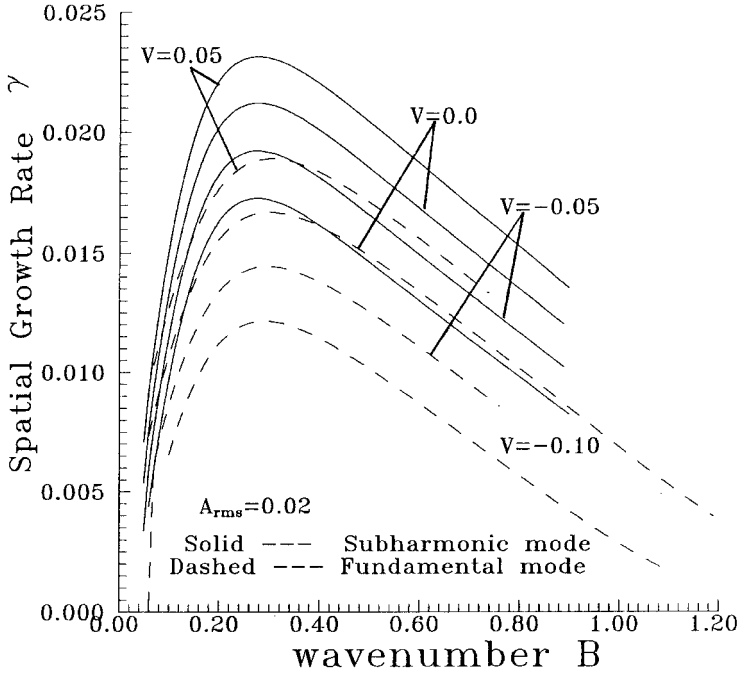

Figure 8. The variation of spatial growth rate γ against wave number B for different suction at $F = 90 * 10^{-6}$ and $Re = 600$.

© 1998 John Wiley & Sons, Ltd.

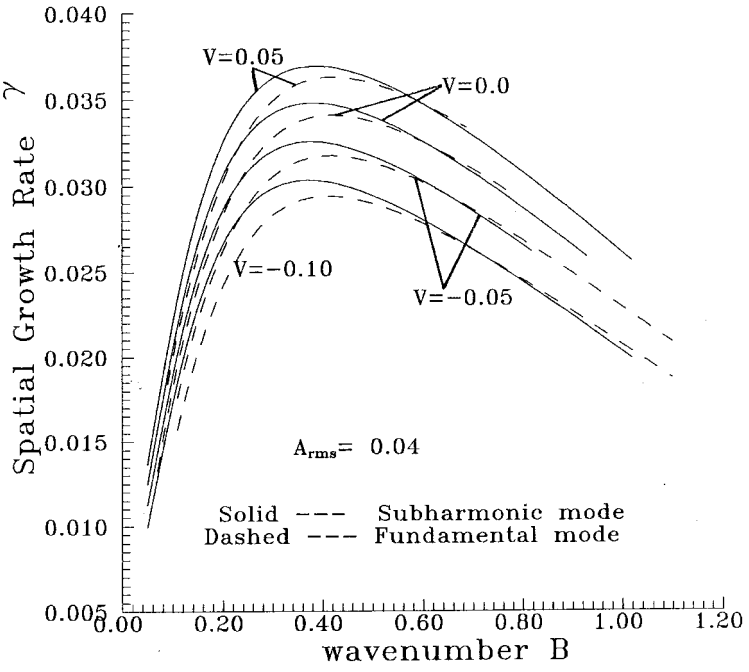

Figure 9. The variation of spatial growth rate γ against wave number B for different suction at $F = 90 * 10^{-6}$ and $Re = 600$.

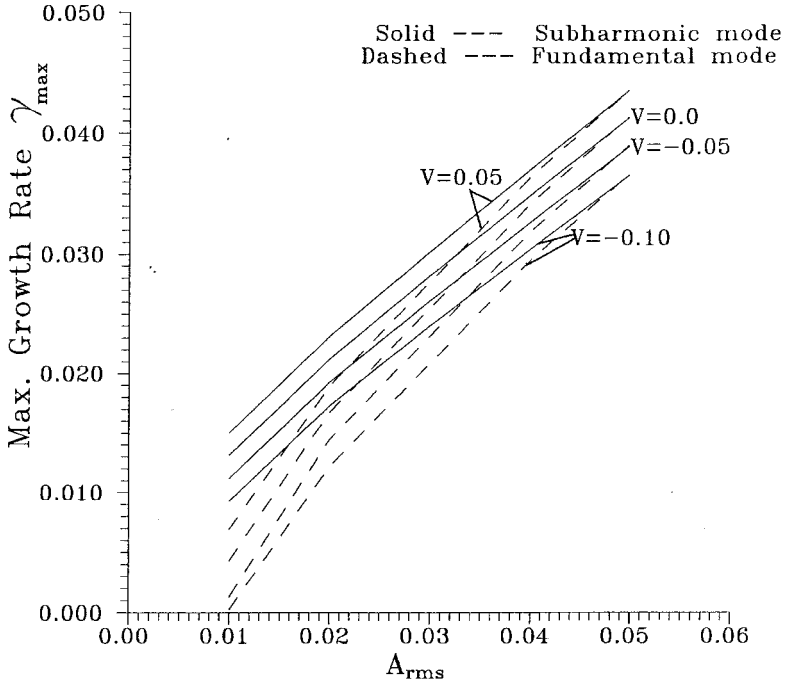

Figure 10. The variation of maximum spatial growth rate γ_{max} against A_{rms} for different V at $F = 90 * 10^{-6}$ and $Re = 600$.

© 1998 John Wiley & Sons, Ltd.

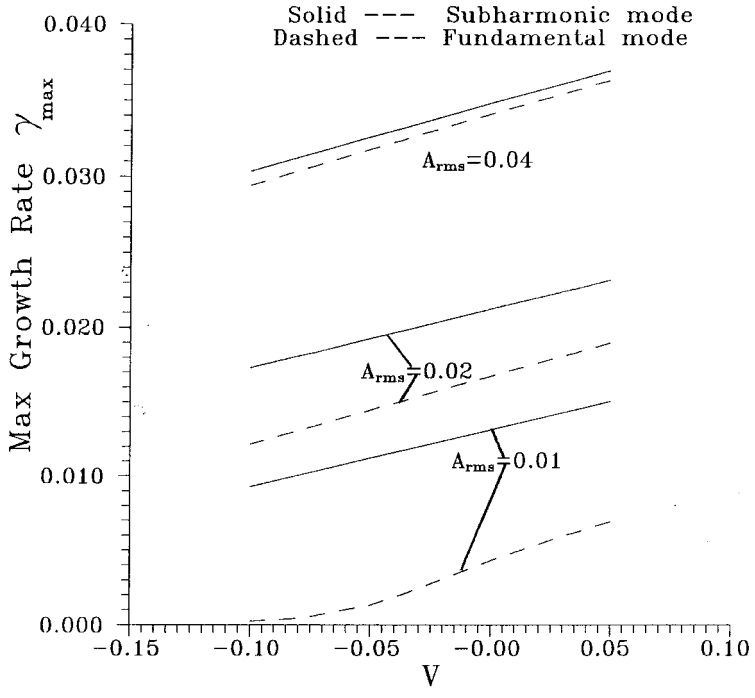

Figure 11. The variation of maximum spatial growth rate γ_{max} against suction V for varied A_{rms} at $F = 90 * 10^{-6}$ and $Re = 600$.

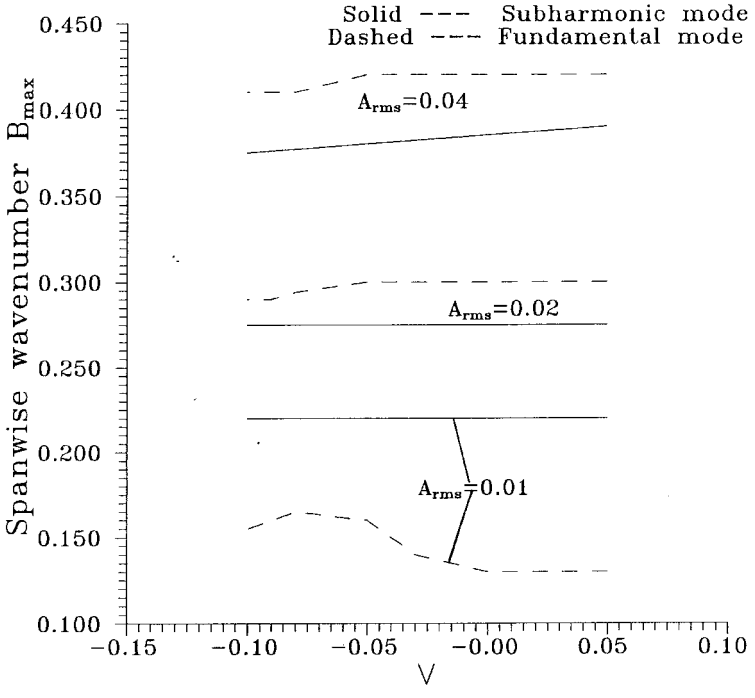

Figure 12. The variation of B_{rms} of the maximum growth rate against V for A_{rms} at $F = 90 * 10^{-6}$ and $Re = 600$.

© 1998 John Wiley & Sons, Ltd.

The present work in analyzing the subharmonic and fundamental instabilities not only provides a good initial guess for DNS, but also offers important information for the verification of results of the DNS approach.

APPENDIX A. COEFFICIENTS FOR SUBHARMONIC MODE

$$F_{12}=1,\qquad F_{21}=Rn\left[\left(\sigma-\frac{i\omega}{2}\right)+U_m\left(\gamma+\frac{i\alpha}{2}\right)\right]-\left(\gamma+\frac{i\alpha}{2}\right)^2+\beta^2,$$

$$F_{23}=Re\,\frac{\mathrm{d}U_m}{\mathrm{d}y},\qquad F_{24}=Re\left(\gamma+\frac{i\alpha}{2}\right),\qquad \bar{F}_{21}=Re\left(\gamma+\frac{i\alpha}{2}\right)u_{\mathrm{p}},$$

$$\bar{F}_{22}=v_{\mathrm{p}}Re,\qquad \bar{F}_{23}=Re\,\frac{\mathrm{d}u_{\mathrm{p}}}{\mathrm{d}y},\qquad G_{21}=Re\left(\gamma+\frac{i\alpha}{2}\right)\bar{u}_{\mathrm{p}},$$

$$G_{22}=\bar{v}_{\mathrm{p}}Re,\qquad G_{23}=Re\,\frac{\mathrm{d}\bar{u}_{\mathrm{p}}}{\mathrm{d}y},\qquad F_{31}=-\left(\gamma+\frac{i\alpha}{2}\right),\qquad F_{35}=-\beta,$$

$$F_{42}=-\left(\gamma+\frac{i\alpha}{2}\right)\Big/Re,\qquad F_{43}=-\left[\left(\sigma-\frac{1}{2}i\omega\right)+U_m\left(\gamma+\frac{i\alpha}{2}\right)\right]+\left[\left(\gamma+\frac{i\alpha}{2}\right)^2-\beta^2\right]\Big/Re,$$

$$F_{46}=-\beta/Re,\qquad \bar{F}_{41}=\left(\gamma-\frac{i3\alpha}{2}\right)v_{\mathrm{p}},\qquad \bar{F}_{43}=-\left(\gamma-\frac{i\alpha}{2}\right)u_{\mathrm{p}}-\frac{\mathrm{d}v_{\mathrm{p}}}{\mathrm{d}y},$$

$$\bar{F}_{45}=v_{\mathrm{p}}\beta,\qquad G_{41}=\left(\gamma+\frac{i5\alpha}{2}\right)\bar{v}_{\mathrm{p}},\qquad G_{43}=-\left(\gamma+\frac{i3\alpha}{2}\right)\bar{u}_{\mathrm{p}}-\frac{\mathrm{d}\bar{v}_{\mathrm{p}}}{\mathrm{d}y},$$

$$G_{45}=\bar{v}_{\mathrm{p}}\beta,\qquad F_{56}=1,\qquad F_{64}=-\beta Re,$$

$$F_{65}=Re\left[\left(\sigma-\frac{i\omega}{2}\right)+U_m\left(\gamma+\frac{i\alpha}{2}\right)\right]-\left(\gamma+\frac{i\alpha}{2}\right)^2+\beta^2,$$

$$\bar{F}_{65}=\left(\gamma-\frac{i\alpha}{2}\right)u_{\mathrm{p}}Re,\qquad \bar{F}_{66}=v_{\mathrm{p}}Re,\qquad G_{65}=\left(\gamma+\frac{i3\alpha}{2}\right)\bar{u}_{\mathrm{p}}Re,$$

$$G_{66}=\bar{v}_{\mathrm{p}}Re,\qquad \hat{G}_{12}=1,\qquad \hat{F}_{21}=\left(\gamma+\frac{i3\alpha}{2}\right)u_{\mathrm{p}}Re,\qquad \hat{F}_{22}=v_{\mathrm{p}}Re,$$

$$\hat{F}_{23}=\frac{\mathrm{d}u_{\mathrm{p}}}{\mathrm{d}y}Re,\qquad \hat{G}_{21}=Re\left[\left(\sigma-\frac{i3\omega}{2}\right)+U_m\left(\gamma+\frac{i3\alpha}{2}\right)\right]-\left(\gamma+\frac{i3\alpha}{2}\right)^2+\beta^2,$$

$$\hat{G}_{23}=Re\,\frac{\mathrm{d}\mathrm{U}_m}{\mathrm{d}y},\qquad \hat{G}_{24}=\left(\gamma+\frac{i3\alpha}{2}\right)Re,\qquad \hat{G}_{31}=-\left(\gamma+\frac{i3\alpha}{2}\right),\qquad \hat{G}_{35}=-\beta,$$

$$\hat{F}_{41}=\left(\gamma-\frac{i\alpha}{2}\right)v_{\mathrm{p}},\qquad \hat{F}_{43}=-\left(\gamma+\frac{i\alpha}{2}\right)u_{\mathrm{p}}-\frac{\mathrm{d}v_{\mathrm{p}}}{\mathrm{d}y},\qquad \hat{F}_{45}=\beta v_{\mathrm{p}},$$

$$\hat{G}_{42}=-\left(\gamma+\frac{i3\alpha}{2}\right)\Big/Re,$$

$$\hat{G}_{43}=-\left[\left(\sigma-\frac{i3\omega}{2}\right)+U_m\left(\gamma+\frac{i3\alpha}{2}\right)\right]+\left[\left(\gamma+\frac{i3\alpha}{2}\right)^2-\beta^2\right]\Big/Re,$$

© 1998 John Wiley & Sons, Ltd.

$$\hat{G}_{46} = -\beta/Re, \qquad \hat{G}_{56} = 1, \qquad \hat{F}_{65} = \left(\gamma + \frac{i\alpha}{2}\right)u_{\mathrm{p}}Re, \qquad \hat{F}_{66} = v_{\mathrm{p}}Re,$$

$$\hat{G}_{64} = -\beta Re, \qquad \hat{G}_{65} = Re\left[\left(\sigma - \frac{i3\omega}{2}\right) + U_m\left(\gamma + \frac{i3\alpha}{2}\right)\right] - \left(\gamma + \frac{i3\alpha}{2}\right)^2 + \beta^2.$$

APPENDIX B. COEFFICIENTS FOR FUNDAMENTAL MODE

$$\tilde{H}_{12} = 1, \qquad \tilde{H}_{21} = Re(\sigma + \gamma U_m) - \gamma^2 + \beta^2, \qquad \tilde{H}_{23} = \frac{\mathrm{d}U_m}{\mathrm{d}y}Re, \qquad \tilde{H}_{24} = \gamma Re,$$

$$\tilde{F}_{21} = \gamma\bar{u}_{\mathrm{p}}Re, \qquad \tilde{F}_{22} = \bar{v}_{\mathrm{p}}Re, \qquad \tilde{F}_{23} = \frac{\mathrm{d}\bar{u}_{\mathrm{p}}}{\mathrm{d}y}Re, \qquad \tilde{F}_{21} = \gamma u_{\mathrm{p}}Re,$$

$$\tilde{\tilde{F}}_{22} = v_{\mathrm{p}}Re, \qquad \tilde{\tilde{F}}_{23} = \frac{\mathrm{d}u_{\mathrm{p}}}{\mathrm{d}y}Re, \qquad \tilde{H}_{31} = -\gamma, \qquad \tilde{H}_{35} = -\beta,$$

$$\tilde{H}_{42} = -\gamma/Re, \qquad \tilde{H}_{43} = -(\sigma + \gamma U_m) + (\gamma^2 - \beta^2)/Re, \qquad \tilde{H}_{46} = -\beta/Re,$$

$$\tilde{F}_{41} = (\gamma + i2\alpha)\bar{v}_{\mathrm{p}}, \qquad \tilde{F}_{43} = -(\gamma + i\alpha)\bar{u}_{\mathrm{p}} - \frac{\mathrm{d}\bar{v}_{\mathrm{p}}}{\mathrm{d}y}, \qquad \tilde{F}_{45} = \beta\bar{v}_{\mathrm{p}}, \qquad \tilde{\tilde{F}}_{41} = (\gamma - i2\alpha)v_{\mathrm{p}},$$

$$\tilde{\tilde{F}}_{43} = -(\gamma - i\alpha)u_{\mathrm{p}} - \frac{\mathrm{d}v_{\mathrm{p}}}{\mathrm{d}y}, \qquad \tilde{\tilde{F}}_{45} = \beta v_{\mathrm{p}}, \qquad \tilde{H}_{56} = 1, \qquad \tilde{H}_{64} = -\beta Re,$$

$$\tilde{H}_{65} = Re(\sigma + \gamma U_m) - \gamma^2 + \beta^2, \qquad \tilde{F}_{65} = (\gamma + i\alpha)\bar{u}_{\mathrm{p}}Re, \qquad \tilde{F}_{66} = \bar{v}_{\mathrm{p}}Re,$$

$$\tilde{\tilde{F}}_{65} = (\gamma - i\alpha)u_{\mathrm{p}}Re, \qquad \tilde{\tilde{F}}_{66} = v_{\mathrm{p}}Re, \qquad F_{12} = 1, \qquad H_{21} = (\gamma + i\alpha)u_{\mathrm{p}}Re, \qquad H_{22} = v_{\mathrm{p}}Re,$$

$$H_{23} = \frac{\mathrm{d}u_{\mathrm{p}}}{\mathrm{d}y}Re, \qquad F_{21} = Re(\sigma - i\omega) + i(\gamma + i\alpha)U_m - ((\gamma + i\alpha)^2 - \beta^2), \qquad F_{23} = \frac{\mathrm{d}U_m}{\mathrm{d}y}Re,$$

$$F_{24} = (\gamma + i\alpha)Re, \qquad G_{21} = (\gamma + i\alpha)\bar{u}_{\mathrm{p}}Re, \qquad G_{22} = \bar{v}_{\mathrm{p}}Re, \qquad G_{23} = \frac{\mathrm{d}\bar{u}_{\mathrm{p}}}{\mathrm{d}y}Re,$$

$$F_{31} = -(\gamma + i\alpha), \qquad F_{35} = -\beta, \qquad H_{41} = (\gamma - i\alpha)v_{\mathrm{p}}, \qquad H_{43} = -\left(\gamma u_{\mathrm{p}} + \frac{\mathrm{d}v_{\mathrm{p}}}{\mathrm{d}y}\right),$$

$$H_{45} = \beta v_{\mathrm{p}}, \qquad F_{42} = -(\gamma + i\alpha)/Re,$$

$$F_{43} = -(\sigma - i\omega) + i(\gamma + i\alpha)U_m + [(\gamma + i\alpha)^2 - \beta^2]/Re, \qquad F_{46} = -\beta/Re,$$

$$G_{41} = (\gamma + i3\alpha)\bar{v}_{\mathrm{p}}, \qquad G_{43} = -(\gamma + i2\alpha)\bar{u}_{\mathrm{p}} - \frac{\mathrm{d}v_{\mathrm{p}}}{\mathrm{d}y}, \qquad G_{45} = \beta\bar{v}_{\mathrm{p}}, \qquad F_{56} = 1,$$

$$H_{65} = \gamma u_{\mathrm{p}}Re, \qquad H_{66} = v_{\mathrm{p}}Re, \qquad F_{64} = -Re\beta,$$

$$F_{65} = Re(\sigma - i\omega) + i(\gamma + i\alpha)U_m - (\gamma + i\alpha)^2 + \beta^2, \qquad G_{65} = (\gamma + i2\alpha)\bar{u}_{\mathrm{p}}Re,$$

$$G_{66} = \bar{v}_{\mathrm{p}}Re, \qquad \hat{G}_{12} = 1, \qquad \hat{F}_{21} = (\gamma + i2\alpha)u_{\mathrm{p}}Re, \qquad \hat{F}_{22} = v_{\mathrm{p}}Re, \qquad \hat{F}_{23} = \frac{\mathrm{d}u_{\mathrm{p}}}{\mathrm{d}y}Re,$$

© 1998 John Wiley & Sons, Ltd.

$$\hat{G}_{21} = Re[(\sigma - i2\omega) + U_m(\gamma + i2\alpha)] - (\gamma + i2\alpha)^2 + \beta^2, \qquad \hat{G}_{23} = \frac{\mathrm{d}U_m}{\mathrm{d}y}$$

$$Re, \qquad \hat{G}_{24} = (\gamma + i2\alpha)Re, \qquad \hat{G}_{31} = -(\gamma + i2\alpha), \qquad \hat{G}_{35} = -\beta, \qquad \hat{F}_{41} = \gamma v_{\mathrm{p}},$$

$$\hat{F}_{43} = -(\gamma + i\alpha)u_{\mathrm{p}} - \frac{\mathrm{d}v_{\mathrm{p}}}{\mathrm{d}y}, \qquad \hat{F}_{45} = \beta v_{\mathrm{p}}, \qquad \hat{G}_{42} = -(\gamma + i2\alpha)/Re,$$

$$\hat{G}_{43} = -[(\sigma - i2\omega) + U_m(\gamma + i2\alpha)] + [(\gamma + i2\alpha)^2 - \beta^2]/Re,$$

$$\hat{G}_{46} = -\beta/Re, \qquad \hat{G}_{56} = 1, \qquad \hat{F}_{65} = (\gamma + i\alpha)u_{\mathrm{p}}Re, \qquad \hat{F}_{66} = v_{\mathrm{p}}Re,$$

$$\hat{G}_{64} = -\beta Re, \qquad \hat{G}_{65} = Re[(\sigma - i2\omega) + U_m(\gamma + i2\alpha)] - (\gamma + i2\alpha)^2 + \beta^2.$$

APPENDIX C. ELEMENT OF MATRIX [B]

At $j = n_{\max}$, the coefficients of the governing equations become constants, so the eigenvalues and the corresponding eigenfunctions are determined analytically. Therefore, the governing equations with constant coefficients are

$$\begin{bmatrix} 1 & 0 & 0 & 0 & 0 & 0 \\ C_{21} & 0 & 0 & C_{24} & 0 & 0 \\ C_{31} & 0 & 0 & 0 & C_{35} & 0 \\ 0 & C_{42} & C_{43} & 0 & 0 & C_{46} \\ 0 & 0 & 0 & 0 & 0 & 1 \\ 0 & 0 & 0 & C_{64} & C_{65} & 0 \end{bmatrix} \begin{Bmatrix} \psi_1 \\ \psi_2 \\ \psi_3 \\ \psi_4 \\ \psi_5 \\ \psi_5 \end{Bmatrix} = \begin{Bmatrix} 0 \\ 0 \\ 0 \\ 0 \\ 0 \\ 0 \end{Bmatrix},$$

The eigenvalues of the system of equations are

$$\chi_{1,2} = \pm\sqrt{C_{21}}, \qquad \chi_{3,4} = \pm\sqrt{C_5 + C_6}, \qquad \chi_{5,6} = \pm\sqrt{C_5 - C_6}.$$

where $C_5 = (C_{24}C_{42} + C_{46}C_{64} + C_{21})/2$ and $C_6 = \sqrt{[C_5^2 + C_{43}(C_{35}C_{64} + C_{24}C_{31})]}$. To obtain elements of the matrix [B], the eigenfunctions of the system adjoining the original system need to be determined first, and the three eigenfunctions corresponding to the negative eigenvalues are used in the determination of elements of [B]. They are

$$\vec{\kappa}_1 = \{\kappa_{11}, \kappa_{12}, \kappa_{13}, \kappa_{14}, \kappa_{15}, \kappa_{16}\}^T = \{1, -1/\chi_2, 0, 0, -C_{24}/C_{64}, C_{24}/\chi_2 C_{64}\}^T,$$

$$\vec{\kappa}_2 = \{\kappa_{21}, \kappa_{22}, \kappa_{23}, \kappa_{24}, \kappa_{25}, \kappa_{26}\}^T$$
$$= \{(C_{21}C_{42} + C_{31}C_{43})/\phi, -(C_{31}C_{43} + C_{42}\chi_4^2)/(\chi_4\phi), -C_{43}/\chi_4, 1, -1(C_{46} + \chi_4\kappa_{26})/C_{64},$$
$$-(C_{24}\kappa_{22} + \chi_4)/C_{64}\}^T, \quad \phi = \chi_4^2 - C_{21},$$

© 1998 John Wiley & Sons, Ltd.

$$\vec{\kappa}_3 = \{\kappa_{31}, \kappa_{32}, \kappa_{33}, \kappa_{34}, \kappa_{35}, \kappa_{36}\}^T$$
$$= \{(C_{21}C_{42} + C_{31}C_{43})/\phi, \ -(C_{31}C_{43} + C_{42}\chi_6^2)/(\chi_6\phi), \ -C_{43}/\chi_6, 1, \ -1(C_{46} + \chi_6\kappa_{26})/C_{64},$$
$$-(C_{24}\kappa_{22} + \chi_4)/C_{64}\}^T, \quad \phi = \chi_6^2 - C_{21},$$

for

$$C_{21} = Re\left[\left(\sigma - \frac{i\omega}{2}\right) + U_m\left(\gamma + \frac{i\alpha}{2}\right)\right] - \left(\gamma + \frac{i\alpha}{2}\right)^2 + \beta^2, \qquad C_{24} = Re\left(\gamma + \frac{i\alpha}{2}\right),$$
$$C_{31} = -\left(\gamma + \frac{i\alpha}{2}\right), \qquad C_{35} = -\beta, \qquad C_{42} = -\left(\gamma + \frac{i\alpha}{2}\right)\Big/ Re,$$
$$C_{43} = -\left[\left(\sigma - \frac{1}{2}i\omega\right) + U_m\left(\gamma + \frac{i\alpha}{2}\right)\right] + \left[\left(\gamma + \frac{i\alpha}{2}\right)^2 - \beta^2\right]\Big/ Re, \qquad C_{46} = -\beta/Re,$$
$$C_{64} = -\beta Re,$$

$$\begin{cases} B_{n1,m1} = \kappa^r_{n,m} & B_{n1,m2} = -\kappa^i_{n,m} \\ B_{n2,m1} = \kappa^i_{n,m} & B_{n2,m2} = -\kappa^r_{n,m} \end{cases}, \qquad \begin{cases} n1 = 2n - 1, & n2 = 2n, & n = 1, 3 \\ m1 = 2m - 1, & m2 = 2m, & m = 1, 6 \end{cases}$$

for

$$\hat{C}_{21} = Re[(\sigma - i2\omega) + U_m(\gamma + i2\alpha)] - \left(\gamma + \frac{i3\alpha}{2}\right)^2 + \beta^2, \qquad \hat{C}_{24} = \left(\gamma + \frac{i3\alpha}{2}\right)Re,$$
$$\hat{C}_{31} = -\left(\gamma + \frac{i3\alpha}{2}\right), \qquad \hat{C}_{35} = -\beta, \qquad \hat{C}_{42} = -\left(\gamma + \frac{i3\alpha}{2}\right)\Big/ Re,$$
$$\hat{C}_{43} = -[(\sigma - i2\omega) + U_m(\gamma + i2\alpha)] + \left[\left(\gamma + \frac{i3\alpha}{2}\right)^2 - \beta^2\right]\Big/ Re, \qquad \hat{C}_{46} = -\beta/Re,$$
$$\hat{C}_{64} = -\beta Re,$$

$$\begin{cases} B_{n1,m1} = \kappa^r_{n,m} & B_{n1,m2} = -\kappa^i_{n,m} \\ B_{n2,m1} = \kappa^i_{n,m} & B_{n2,m2} = -\kappa^r_{n,m} \end{cases}, \qquad \begin{cases} n1 = 2n - 1 + 6, & n2 = 2n + 6, & n = 1, 3. \\ m1 = 2m - 1 + 6, & m2 = 2m + 6, & m = 1, 6. \end{cases}$$

REFERENCES

1. D.M. Bushnell and J.N. Hefner, 'Viscous drag reduction in boundary layers', in *AIAA Progress in Astronautics and Aeronautics Series*, *Vol. 123*, AIAA, New York, 1990.
2. P.S. Klebanoff and K.D. Tidstrom, 'The three dimensional nature of boundary layer instability', *J. Fluid Mech.*, **12**, 1–34 (1962).
3. Y.S. Kachanov and V.Y. Levchenko, 'The resonant interaction of disturbances at laminar turbulent transition in a boundary layer', *J. Fluid. Mech.*, **138**, 209–247 (1984).
4. A.S.W Thomas and W.S Saric, 'Harmonic and subharmonic waves during boundary-layer transition', *Bull. Amer. Phys. Soc.*, **26**, 1252 (1981).
5. W.S. Saric and A.S.W. Thomas, 'Experiments on the subharmonic route to turbulence in boundary layers', in T. Tatsumi (ed.), *Turbulent and Chaotic Phenomena in Fluids*, North-Holland, Amsterdam, 1990, pp. 117–122.
6. P.R. Spalart and K.S. Yang, 'Numerical simulation of boundary layers: Part 2. Ribbon-induced transition in boundary layer', *NASA Technical Memorandum 88221*, 1–24 (1986).

© 1998 John Wiley & Sons, Ltd.

7. L. Kleiser and E. Laurien, 'Three-dimensional numerical simulation of laminar turbulent transition and its control by periodic disturbances', in V.V. Kozlov (ed.), *Laminar-Turbulent Transition*, Springer, Berlin, Heidelberg, 1985, pp. 29–37.
8. Th. Herbert, 'Analysis of the subharmonic route to transition in boundary layers', *AIAA Paper 84-0009*, 1984.
9. Th. Herbert, 'Three-dimensional phenomena in the transitional flat-plate boundary layer', *AIAA Paper 85-0489*, 1985.
10. Th. Herbert, 'Secondary instability of boundary layer', *Ann. Rev. Fluid Mech.*, **20**, 487–526 (1988).
11. Th. Herbert and F.P. Bertolotti, 'Effect of pressure gradients on the growth of subharmonic disturbances in boundary layers', in T.J. Mueller (ed.), *Proc. Conf. on Low Reynolds Number Airfoil Aerodynamics*, University of Notre Dame, 1985.
12. N.M. EI-Hady, 'Effect of suction on controlling the secondary instability of boundary layers', *Phys. Fluids A*, **3**, 393–402 (1991).
13. J.A. Masad and A.H. Nayfeh, 'Effects of suction on wall shaping on the fundamental parametric resonance in boundary layers', *Phys. Fluids A*, **4**, 963–974 (1992).
14. F.P. Bertolotti, 'Temporal and spatial growth of subharmonic disturbances in falkner skan flows', *M.Sc. Thesis*, Virginia Polytech. Institute State University, Blacksburg, 1987.
15. M.R. Scott and H.A. Watts, 'Computational solution of two-point boundary value problems via orthonormalization', *SIAM J. Numer. Anal.*, **14**, 40 (1977).
16. V. Pereyra, 'An adaptive finite-difference FORTRAN program for first order nonlinear boundary value problem', in *Lecture Notes in Computer Science* 76, Springer, Berlin, PASVA3, 1978, pp. 67–88.
17. G.R. Santos, 'Studies of secondary instability', *Ph.D. Dissertation*, Va. Polytech. Inst. State Univ., Blacksburg, 1987.
18. J.L. Wu, 'Instability of a compressible mixing layer', *Ph.D. Dissertation*, Va. Polytech. Inst. State Univ., Blacksburg, 1989.
19. Patel, A, Vithal, *Numerical Analysis*, Harcourt Brace College, Orlando, Florida, 1994.

© 1998 John Wiley & Sons, Ltd.